

## Supplementary Information

J. B. J. Chapman,<sup>1,2</sup> O. T. Gindele,<sup>1,2</sup> C. Vecchini,<sup>2</sup> P. Thompson,<sup>3,4</sup>  
M. Stewart,<sup>2</sup> M. G. Cain,<sup>5</sup> D. M. Duffy,<sup>1</sup> and A. Kimmel<sup>1</sup>

<sup>1</sup>*Department of Physics and Astronomy, University College London, Gower Street, London WC1E 6BT, UK*

<sup>2</sup>*National Physical Laboratory, Hampton Road, Teddington, TW11 0LW, UK*

<sup>3</sup>*XMaS, The UK-CRG, ESRF, BP 220, F-38043 Grenoble CEDEX, France*

<sup>4</sup>*Department of Physics, University of Liverpool, Liverpool, L69 3BX, UK*

<sup>5</sup>*Electrosiences Ltd, 1 Osborn Road, Farnham, GU9 9QT, UK*

(Dated: June 29, 2017)

### A. Further Simulation Details

The local polarization of the molecular dynamics simulations was calculated using the method of Sepiarsky and Cohen [1]: A conventional ( $\text{A}_8\text{BO}_6$ ) unit cell is defined by the B-cation within its oxygen octahedron, surrounded by the eight nearest Pb neighbours. For charge neutrality of the conventional cell the charges of O and Pb atoms are normalized by a factor ( $w$ ) of 2 and 8, respectively. Taking the core position of the B-cation ( $r_B$ ) as a reference point, the effective polarization,  $P$ , for such a cell is calculated as:

$$P = \frac{1}{v} \sum_i \frac{1}{w_i} q_i (r_i - r_B).$$

Here,  $v$  is the volume of a conventional unit cell,  $i$  is the atom index,  $q_i$  and  $r_i$  are the charges and positions of particle  $i$ . Averaging over all conventional unit cells of the systems gives the macroscopic polarization.

### B. Further Experimental Details

The ceramic samples (PC5H) used in the experimental setup 1 were 10mm diameter discs of 1mm thickness, with silver fired electrodes. Setup 2 used the Fuji-c91 material with electroplated nickel electrodes, a thickness of 0.15 mm and cross sectional area 5 mm by 10 mm. Each sample was mounted onto a sapphire disk, with an evaporated gold strip coated on one side of the disk with conductive silver paint. The sapphire disk was then mounted with conductive silver paint onto the cold finger of a cryostat (Advanced Research Systems DE202 closed cycle cryocooler). The temperature of the sample was measured by a Cernox sensor, embedded into the cold finger below the sample and a Lakeshore model 340 temperature controller controlled the sample temperature to a stability of less than 10mK. Supply and return wires to and from the sample were terminated using conductive silver paint. A separate measurement point at 77K was made (in liquid nitrogen) using the Fuji material using a slightly different setup (setup 2) that permitted higher electric fields to be applied.

From the experiments, polarisation ( $P = \epsilon_0 E + D$ ) where  $D = Q/A$  was calculated from charge,  $Q$ , measured as a function of time (current,  $I = \partial Q/\partial t$ ) using a modified Sawyer-Tower or virtual earth instrumentation amplifier, and area,  $A$ , of the collection plates, as described in [2]. In order to eliminate the effects arising from the history of electrical loading on the sample we used electrical conditioning of the device under test. Here, a cyclical electric field with its amplitude decreasing over time was applied to establish a gradual de-poling of the material. This ensured a symmetrical polarization response for the next measured cycle.

### C. Additional Forcefield Validation

#### *Domain Wall Energy*

The CP2K package [3] is used to study rocksalt (P4mm) PZT from density functional theory. Large  $6 \times N \times 6$  (with  $N=6,8,10,12$ ) supercells were constructed allowing for  $\Gamma$ -point only k-point calculations. We use an energy cutoff of 600 Ry and a relative energy cut-off of 60 Ry. The PBEsol exchange correlation functional [4] was implemented with PBE-GTH pseudopotentials [5] and MOLOPT basis sets [6]. Calculations of  $\text{PbTiO}_3$  and PZT, excluding domain

walls, were additionally performed producing lattice parameters and electronic structures within 1% agreement with the planewave density functional theory calculations used to derive the forcefield. Supercells were constructed to include  $180^\circ$  and  $90^\circ$  domain walls and relaxed using geometry optimization. Domain wall energies are then calculated as the energy difference between the monodomain  $E_{bulk}$  and polydomain  $E_{Domain}$  system, normalized by the total domain wall area:

$$E_{DW} = \frac{E_{Bulk} - E_{Domain}}{2A} \quad (1)$$

Molecular dynamics simulations incorporating domain walls are computationally cheaper enabling much larger simulation cells.  $180^\circ$  and  $90^\circ$  domain walls of rocksalt PZT were calculated at 10 K in an NPT ensemble. For the MD runs, domain wall separations are  $115 \text{ \AA}$  and  $630 \text{ \AA}$  for the  $90^\circ$  and  $180^\circ$ , respectively. The domain wall separation is increased to show convergence (Figure 1).

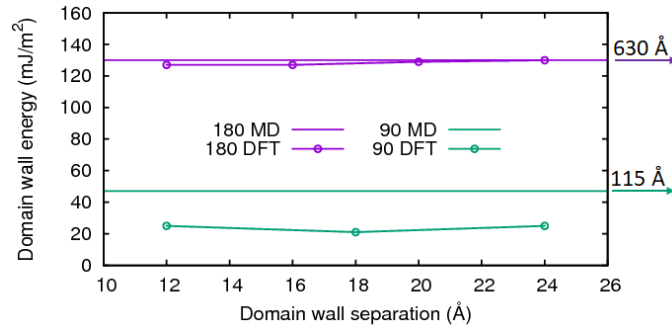


FIG. 1: Stability of  $180^\circ$  and  $90^\circ$  domain walls in  $P4mm$   $PbZr_{0.5}Ti_{0.5}O_3$  determined via geometry optimization within the density functional theory framework and molecular dynamics (MD) implementing a core-shell forcefield. MD values correspond to domain wall separations of  $115 \text{ \AA}$  and  $630 \text{ \AA}$  for  $90^\circ$  and  $180^\circ$  walls, respectively. Domain wall energy calculated as the relative energy difference between the monodomain bulk  $E_{Bulk}$  and the system including domain walls  $E_{Domain}$ , normalized by the domain wall area:  $E_{DW} = (E_{Bulk} - E_{Domain})/2A$ .

#### Field Driven Transition

Experiments on nominally rhombohedral PZT have identified an  $R \rightarrow M_A \rightarrow T$  transition from an  $[001]$  applied electric field [7]. We simulate a composition of  $PbZr_{0.55}Ti_{0.45}O_3$  which has a rhombohedral groundstate and near the MPB to match the experiment. Performing MD using an  $N\sigma T$  ensemble and applying an electric field along  $[001]$  we observe a field-driven transition sequence in agreement with experiment justifying the forcefield (Figure 2).

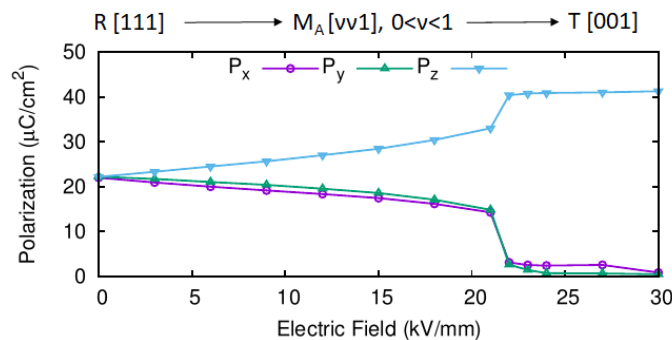


FIG. 2: Polarization components of rhombohedral  $PbZr_{0.55}Ti_{0.45}O_3$  as a function of the magnitude of applied field along  $[001]$  at 50 K.

## D. Supplementary Results

### 1. $60 \times 20 \times 60$ Convergence Test

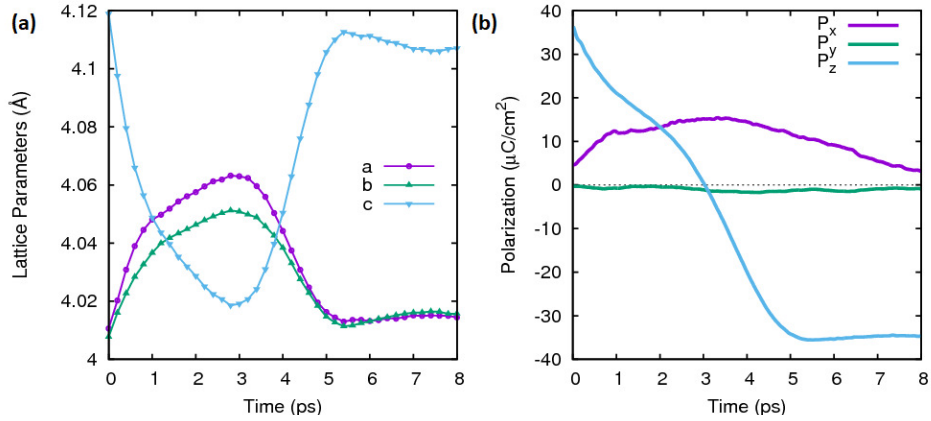


FIG. 3: Lattice parameters (a) and polarization components (b) of  $\text{PbZr}_{0.5}\text{Ti}_{0.5}\text{O}_3$  at 100 K. Calculated using a  $60 \times 20 \times 60$  supercell. Results are consistent with the smaller cell simulations reported in the main manuscript.

### $\text{PbZr}_{0.2}\text{Ti}_{0.8}\text{O}_3$ Phase Transition Sequence and Switching

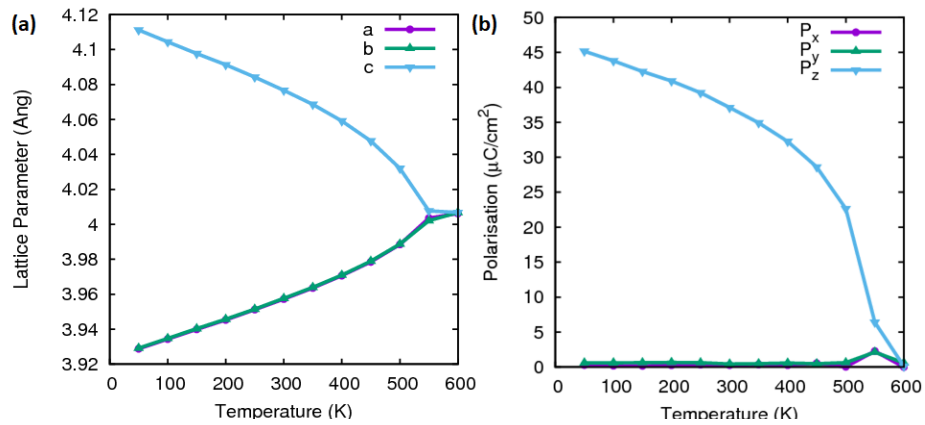


FIG. 4: (a) Lattice parameters and (b) polarization temperature driven phase transition of  $\text{PbZr}_{0.2}\text{Ti}_{0.8}\text{O}_3$ .

- 
- [1] M. Sepliarsky and R. E. Cohen, *Journal of Physics: Condensed Matter* **23**, 435902 (2011).
  - [2] J. Wooldridge, S. Ryding, S. Brown, T. L. Burnett, M. G. Cain, R. Cernik, R. Hino, M. Stewart, and P. Thompson, *Journal of Synchrotron Radiation* **19**, 710 (2012).
  - [3] J. VandeVondele, M. Krack, F. Mohamed, M. Parrinello, T. Chassaing, and J. Hutter, *Computer Physics Communications* **167**, 103 (2005).
  - [4] J. P. Perdew, A. Ruzsinszky, G. I. Csonka, O. A. Vydrov, G. E. Scuseria, L. A. Constantin, X. Zhou, and K. Burke, *Physical Review Letters* **100**, 136406 (2008).
  - [5] S. Goedecker, M. Teter, and J. Hutter, *Physical Review B* **54**, 1703 (1996).
  - [6] J. VandeVondele and J. Hutter, *Journal of Chemical Physics* **127**, 114105 (2007).
  - [7] R. Guo, L. E. Cross, S. E. Park, B. Noheda, D. E. Cox, and G. Shirane, *Physical Review Letters* **84**, 5423 (2000).